

Novel planar transmission line coupling elements for use in deployable antenna systems

Alan Thompson⁽¹⁾, Martin S. Thompson⁽²⁾

⁽¹⁾Eureco Technologies Ltd, 2 Puckpool Hill, Ryde, Isle of Wight, PO33 1PJ, UK, Email: a.thompson@eureco.com

⁽²⁾Eureco Technologies Ltd, Email: m.thompson@eureco.com

ABSTRACT

Beam-forming network (BFN) losses can severely limit the efficiency of very large aperture direct radiating array (DRA) antennas. At low frequencies, the BFN typically uses coaxial cable technology but launch vehicle, stowage and deployment requirements impose design constraints that exacerbate BFN losses. Other issues include excessive resistive torque and passive intermodulation (PIM). Novel planar transmission line coupling elements have been conceived to circumvent these issues. Computed S-parameter results are presented, applications identified and future activities outlined.

1. INTRODUCTION

In its simplest form, a direct radiating array (DRA) comprises an array of radiating elements that are excited by means of a beam forming network (BFN). A passive array configuration is desirable for very large apertures but losses in the BFN can severely limit the DRA efficiency. For example, in a P-band synthetic aperture radar (SAR) mission requiring an antenna aperture greater than 22m, the losses in a coaxial cable BFN could exceed 3dB. Such high losses impact the requirements of the payload transmitter and make greater demands on the DC power conditioning, battery and solar panel subsystems of the satellite. Furthermore in P-band, since the International Telecommunication Union (ITU) Recommendations ITU-R SA.1260-1 limit the power flux density at the surface of the Earth, the reduced antenna efficiency limits the Noise Equivalent Sigma Nought (NESN), a measure of the sensitivity of the SAR instrument, thus compromising the scientific return of a P-band SAR mission. At relatively low frequencies, such as P-band and L-band, the need for a physically large aperture in either a SAR or telecommunication mission, generally leads to a trade-off between a large passive DRA and a large deployable reflector. Since the beginning of the 1980s, although active DRAs were often originally considered for several programmes, the solutions selected from a detailed technical and economical trade-off, have mostly been based on mechanically steerable reflector antennas. Nevertheless, with the ability to control the amplitude and phase of the radiating elements or subarrays, the DRA antenna configuration offers the best flexibility for radar and telecommunication space missions. Innovative architectures and technologies are

therefore needed to overcome the large number of constraints associated with DRAs before their acceptance can be realised at an affordable cost [1].

In a design effort to overcome issues of high resistive deployment torque, excessive loss, phase instability and passive intermodulation (PIM), which are associated with coaxial cable harnesses, novel planar transmission line coupling elements were conceived. The coupling elements allow radio frequency continuity at the inter-panel junctions of large deployable panels, which are based on low density foam or honeycomb dielectric spacers, to form low frequency DRAs with excellent mechanical and electrical performance. The introduction of the coupling elements in this paper is aimed at stimulating discussions with parties who are interested in developing this new connective technology for a variety of DRA and other space technologies.

2. RADIO FREQUENCY HARNESS ISSUES IN DEPLOYABLE ANTENNAS

A radio frequency (RF) harness, comprising a large number of long coaxial cables, is typically used as part of a BFN to make signal path connections between transmit/receive (TR) modules, located in a central region of a satellite, and subarrays of radiating elements distributed across the large aperture of a low frequency antenna. The flexible ultra-low-loss coaxial cable Type SHF2.4M (outer diameter 2.45 mm), manufactured by Radiall, is taken as a benchmark, since this coaxial cable is state-of-the-art and it has been used in the BIOMASS P-band radar studies [2]. RF harness issues are associated with the following parameters:

- Attenuation
- Phase stability
- Passive intermodulation
- Resistive torque
- Mass

For coaxial cable, having the same type of construction and materials, the attenuation due to conductor losses is inversely proportional to the diameter of its dielectric and directly proportional to the square root of frequency. Dielectric loss is independent of the cable diameter and is directly proportional to frequency. In P-band, the total attenuation of Type SHF2.4M coaxial cable is 0.388dB/m. The larger diameter coaxial cable

Type SHF5 (jacket diameter 5.25mm), would reduce the attenuation to 0.169 dB/m but it would have a much higher flexural stiffness.

The phase stability of a coaxial cable is critically dependent on its form of construction and materials content. For Type SHF2.4M cable, the phase stability with bending is $<0.4^\circ/360^\circ / \text{GHz}$ and the phase stability with temperature is $<3^\circ/\text{m}/\text{GHz}$ (-55°C to $+100^\circ\text{C}$).

Passive intermodulation (PIM) products, caused by metal-to-metal contact, can be produced at the coaxial connectors and along the lengths of braided coaxial cable that feed subarrays in an antenna [3, 4]. Special connectors and assembly procedures are required to meet demanding PIM requirements. PIM interference can have a serious impact on the performance of high-power multi-frequency telecommunication systems, especially when the antenna is shared by the transmitter and the receiver at the same time.

The resistive torque of a RF cable harness becomes an issue when the cable diameter and the number of cables are increased. Tests performed on a group of twelve Type SHF2.4M cables showed that the resistive torque was too high at 0.58 Nm [5]. Although the resistive torque of this group of cables was reduced to 0.27 Nm by means of a cable drum, there are possible issues for deployment actuators when the RF harness comprises a much larger number of coaxial cables.

The mass of Type SHF2.4M cable is 14 g/m. For a large P-band deployable antenna, the total cable length is several hundred metres and the combined mass of the cables and drums is >10 kg. If the lower loss cable Type SHF5 were to be used, the combined mass would increase to >50 kg. Neither the cables nor the cable drums contribute to the stiffness of the antenna.

3. STEPPED APERTURE DRA

The accommodation, deployment and operation of a large low frequency radar system, such as a P-band SAR, present numerous design constraints and challenges. A stepped-aperture DRA, which potentially offers performance benefits, as well as economic, mechanical and electrical advantages, was conceived in response to these challenges [6, 7, 8]. In principle the folded stepped-aperture array can be accommodated within the fairing envelope of a Vega launch vehicle and provides a radiating surface area of 74m^2 when deployed (Fig. 1). The stepped-aperture array is based on a deployable panel structure comprising sets of panels that are hinged together about spaced-apart axes, some of which being transverse and others being parallel to an elongate axis. Subarrays of radiating elements are fed by means of planar transmission lines, either in microstrip or stripline, which are an integral

part of the panel structure, thus contributing stiffness to each panel of the resulting antenna.

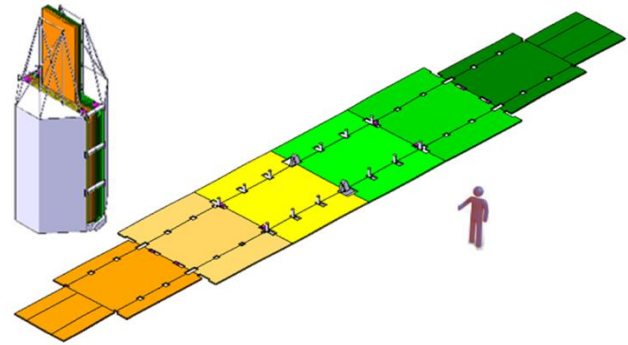
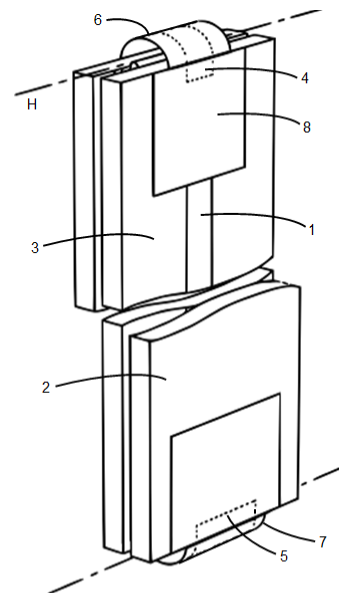


Figure 1. A stepped-aperture array in the stowed and deployed states.

4. BRIDGING THE GAPS

The planar transmission line coupling elements were invented to provide a means of bridging the gaps at the inter-panel junctions of the stepped-aperture DRA panels, without resorting to RF harnesses and thus avoid the issues described above. Details of the invention have been disclosed in a patent application [9].

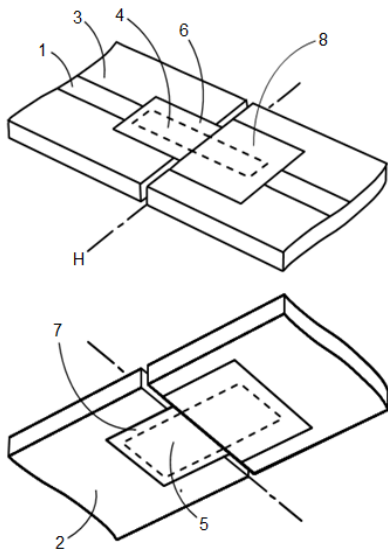
Fig. 2 shows folded sections of microstrip transmission line, each comprising a trace and a ground plane separated by a dielectric substrate in the normal manner. In this stowed state, flexible dielectric bridges, containing either a flexible trace or a flexible ground plane, are seen arched at the inter-panel junctions.



1 Trace; 2 Ground plane; 3 Dielectric substrate; 4 Flexible trace; 5 Flexible ground plane; 6 Flexible trace dielectric; 7 Flexible ground dielectric; 8 Dielectric guide cover; H Hinge axis

Figure 2. A three-section microstrip transmission line folded about two axes in a stowed state.

During the deployment phase, the flexible dielectric bridges unfold and slide over their respective traces and ground planes until the deployed state is reached, as shown in Fig. 3. In this deployed state, the flexible trace, which is separated from each microstrip trace by a dielectric medium, forms two series-branching [10] low-impedance parallel-plate transmission lines, which are nominally a quarter-wavelength long at the operating frequency. Similarly, the flexible ground plane, which is separated from each microstrip ground plane by a dielectric medium, forms series-branching low-impedance microstrip transmission lines, which are nominally a quarter-wavelength long at the operating frequency.



1 Trace; 2 Ground plane; 3 Dielectric substrate; 4 Flexible trace; 5 Flexible ground plane; 6 Flexible trace dielectric; 7 Flexible ground dielectric; 8 Dielectric guide cover; H Hinge axis

Figure 3. Two aspects of a two-section microstrip transmission line in an unfolded deployed state.

A simplified equivalent circuit of the coupling elements bridging a gap in a two-section planar transmission line is shown in Fig.4. The planar transmission line, in either microstrip or stripline form, is of characteristic impedance Z_0 . The characteristic impedance of each series-branching line is very much less than that of the planar transmission line. Each series-branching transmission line (also known as a series stub) is terminated in an open circuit, which is transformed to a short circuit at each bridge abutment by means of the impedance inverter property of the quarter-wavelength line. Each short circuit (or very low impedance) provides RF continuity for the respective flexible traces and flexible ground planes to facilitate a bridging planar transmission line connection between the adjacent sections of planar transmission line.

Since metal-to-metal contact is avoided in the coupling elements, PIM prevention should be achieved if PIM

prevention rules are followed for other parts and components of the antenna subsystem.

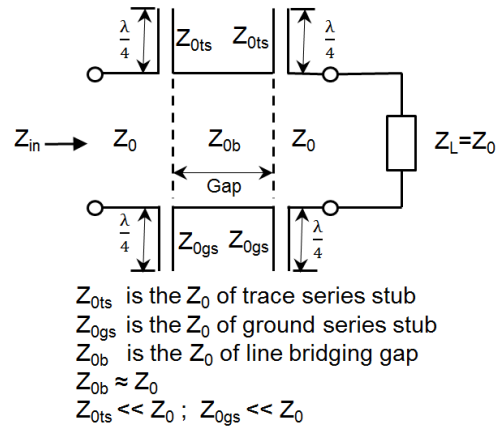


Figure 4. A simplified equivalent circuit of the coupling elements bridging a gap in a two-section planar transmission line.

5. SCATTERING PARAMETER PLOTS

MATLAB and the RF Toolbox were used to analyse the simplified equivalent circuit of Fig. 4 to produce plots of scattering parameters $|S_{11}|$ and $|S_{21}|$ vs frequency for microstrip coupling elements to give an insight into their behaviour. Stripline coupling elements are expected to exhibit a similar behaviour. The results of the computation for respective sets of coupling element dimensions are shown in Fig. 5 and Fig. 6 for the ultra-high frequency satellite communication band (UHF SATCOM), P-band SAR (Fig. 7 and Fig. 8), L-band SAR (Fig. 9 and Fig. 10) and S-band SAR (Fig. 11 and Fig. 12).

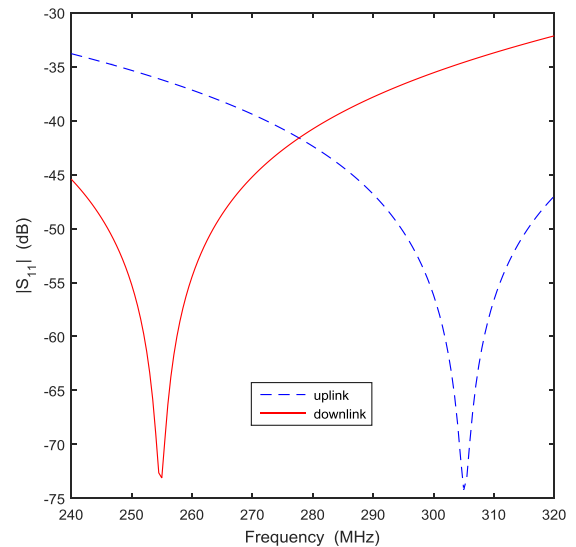


Figure 5. Computed scattering parameters $|S_{11}|$ vs frequency for the coupling elements in the UHF SATCOM band.

Although the simplified equivalent circuit (Fig. 4) provides a useful insight into the behaviour of the reflection and transmission characteristics of the coupling elements, the results of such analysis do not include radiation loss or the effects of evanescent modes. Nevertheless, the results of a preliminary model using the finite element method (FEM) show similar characteristics for the scattering parameters and very little radiation from the coupling elements.

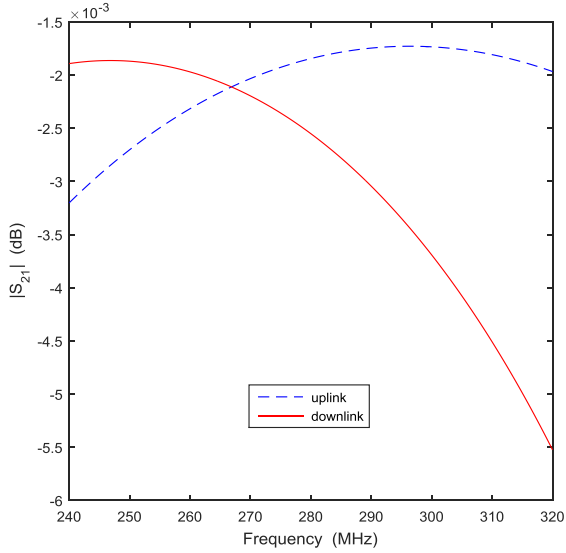


Figure 6. Computed scattering parameters $|S_{21}|$ vs frequency for the coupling elements in the UHF SATCOM band.

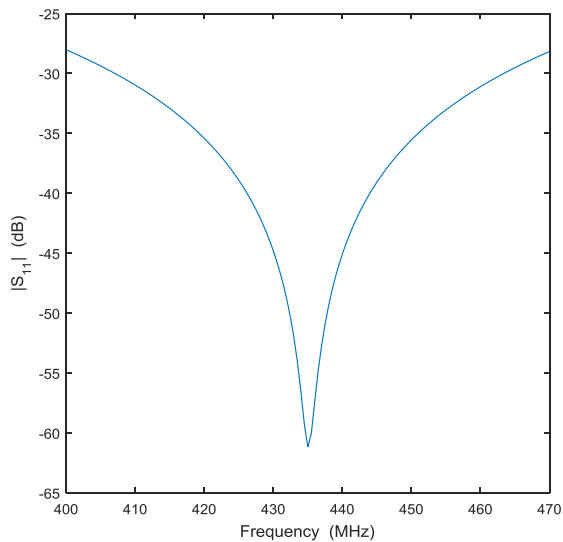


Figure 7. Computed scattering parameter $|S_{11}|$ vs frequency for the coupling elements in P-band.

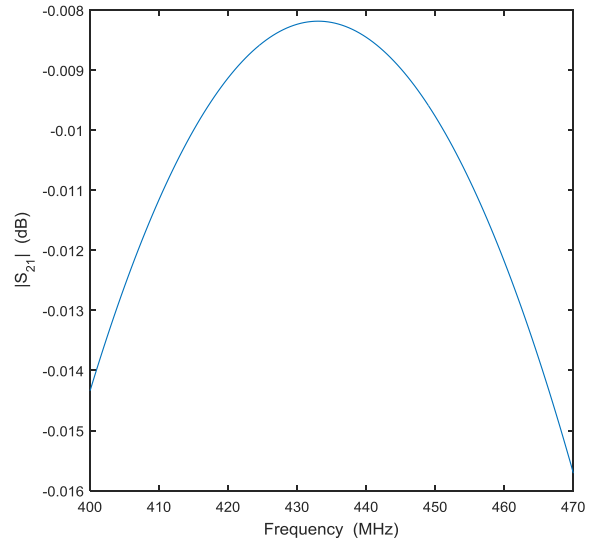


Figure 8. Computed scattering parameter $|S_{21}|$ vs frequency for the coupling elements in P-band.

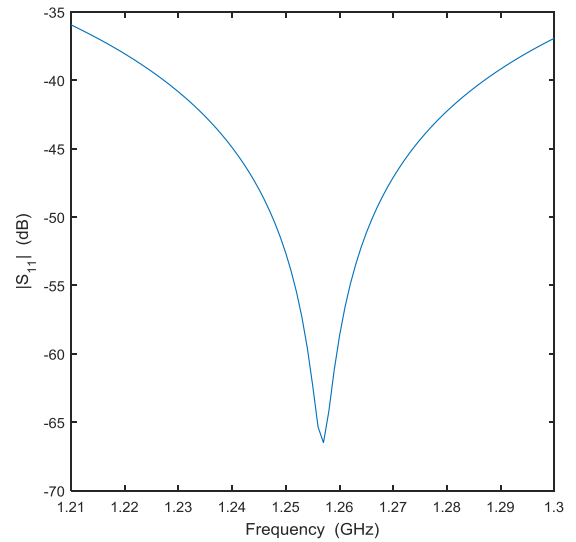


Figure 9. Computed scattering parameter $|S_{11}|$ vs frequency for the coupling elements in L-band.

Tab. 1 summarises the computed insertion loss of the coupling elements and the attenuation of their respective planar transmission lines. A software tool [11, 12] was used to calculate the attenuation of microstrip and stripline planar transmission lines, which are based on the use of a foam dielectric substrate, having a relative permittivity of 1.06 and a loss tangent of 0.0002, and of copper conductors for the trace and ground plane. The dimensions of the transmission lines and the coupling elements were selected to suit sample applications in each of the frequency bands.

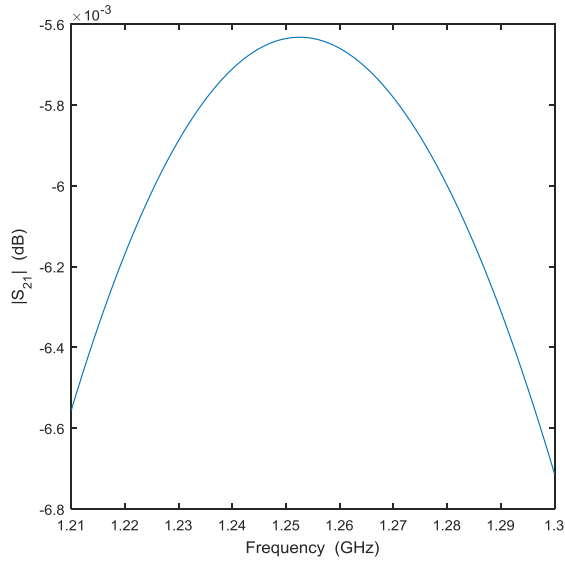


Figure 10. Computed scattering parameter $|S_{21}|$ vs frequency for the coupling elements in L-band.

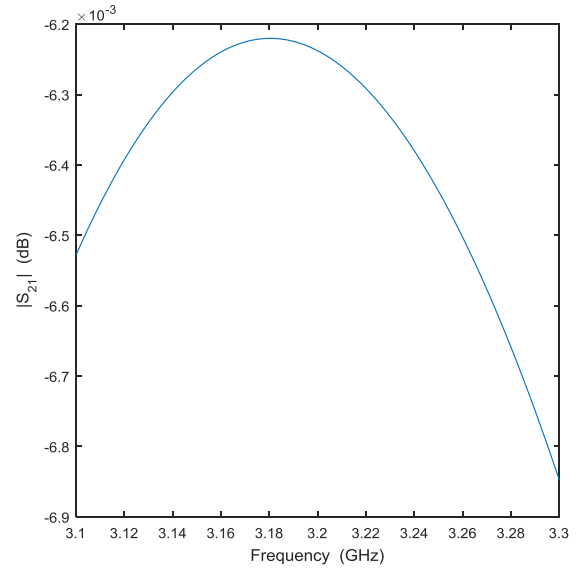


Figure 12. Computed scattering parameter $|S_{21}|$ for the coupling elements in S-band.

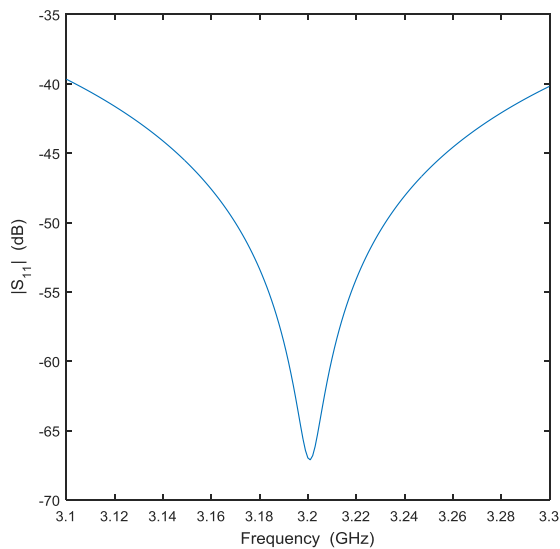


Figure 11. Computed scattering parameter $|S_{11}|$ vs frequency for the coupling elements in S-band.

Table 1. A summary of the calculated insertion loss of the coupling elements and attenuation of their respective planar transmission lines. The attenuation of Type SHF2.4M coaxial cable is included for comparison.

Band	Coupling element insertion loss dB	Microstrip attenuation dB/m	Stripline attenuation dB/m	Type SHF2.4M attenuation dB/m
UHF	0.002	0.008	0.009	0.345
P	0.008	0.025	0.024	0.388
L	0.007	0.051	0.051	0.707
S	0.007	0.163	0.147	1.137

6. DELAY AND PHASE CHARACTERISTICS

Fig. 13 shows the computed phase angle of the scattering parameter S_{21} vs frequency for the coupling elements in L-band. The phase is seen to vary linearly with frequency, implying that a constant true time delay (TTD) is introduced throughout the frequency band. The group delay is $1.2809e-10$ s, of which $6.6713e-11$ s is attributed to an inter-panel gap of 20mm, which was used in the computer model, and $6.1377e-11$ s is attributed to the series-branching low impedance lines.

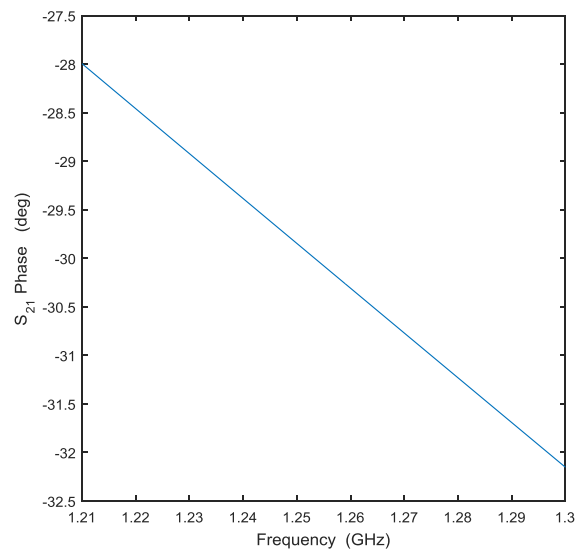


Figure 13. Computed phase angle of the scattering parameter S_{21} vs frequency for the coupling elements in L-band.

7. SPACE APPLICATIONS

Potential space applications for the planar transmission line coupling elements are mostly in the lower frequency bands, where the RF structure of an antenna serves also as a mechanical support to give an efficient utilisation of mass [13]. The very low losses offered by the combination of coupling elements and planar transmission lines through to L-band, may make it unnecessary to place transmit/receive modules (TRMs) on deployable panels in these frequency bands, which could give technical and cost-saving benefits. A centralised location of the electronic subsystems would facilitate an easier implementation of digital beam forming (DBF) techniques, bringing advantages for meeting demanding mission requirements. Some space applications that may benefit from the use of the proposed coupling elements in their respective payload antenna subsystems are identified for different frequency bands in the following subsections.

7.1. VHF band

The very high frequency (VHF) band was the first to be used in space by the Sputnik series of satellites in 1957/8 for telemetry tracking and command (TT&C). More recently, a satellite-based Automatic Identification System (AIS), operating at a frequency of 165 MHz, has been developed for the automatic exchange of navigational data between ships, coastal stations and satellites [14]. By using the coupling elements to assist the deployment of antenna elements from a small satellite, a higher gain antenna could give improved system performance.

7.2. UHF band

The UHF SATCOM frequency band is favoured for reliably penetrating jungle foliage, inclement weather and urban terrain. Large deployable mesh reflector antennas currently dominate this domain but, by using the proposed coupling elements, deployable high-efficiency DRAs could give improvements in system performance and operational flexibility

7.3. P-band

Variants of DRAs were initially favoured by industry to meet the original scientific requirements of the BIOMASS mission. Following a relaxation of the mission requirements, a deployable mesh reflector antenna was selected.

Future Earth Observation missions in P-band are likely to require DRAs to produce reconfigurable beams in response to exacting scientific requirements for ice-sheet sub-surface mapping of the Polar Regions [15]. The predicted performance of the coupling elements is compatible with the requirements of a possible extended frequency band, e.g. 400-470 MHz, on a secondary

basis for the non-populated Antarctic region.

The NESN represents the backscattering coefficient that is equivalent to the background noise in the SAR image. If the NESN is not sufficiently low, e.g. due to excessive loss in the BFN, then the retrieval of lower biomass values and the mapping of subsurface geomorphology in arid zones are compromised [16]. An excessively high NESN also degrades the quality of interferometric measurements by reducing coherence.

A high-efficiency DRA antenna, realised by using low-loss, phase-stable planar transmission line in conjunction with the proposed coupling elements to feed the subarrays and combined with DBF techniques, would give a lower NESN and permit a higher azimuth resolution over a wider swath [17].

7.4. L-band

Special applications of the global navigation satellite system (GNSS) may benefit from passive reception by means of deployable DRA antennas, based on the use of the proposed coupling elements, for realising beam steering, tracking, low-multipath and interferometry.

Ocean surface wide-swath altimetry using GNSS reflected (GNSS-R) signals [18] could benefit from the use of a high-efficiency, multi-beam DRA antenna that would allow a larger number of simultaneous reflections to be received. A deployable form of such a DRA antenna, using the coupling elements, could allow its accommodation on a small satellite to permit a low-cost launch.

The MIRAS (Microwave Imaging Radiometer with Aperture Synthesis) instrument, used in the Soil Moisture and Ocean Salinity (SMOS) mission, has a Y-shaped limb configuration with equally spaced antenna elements, each polarisation directly feeding a low noise amplifier (LNA) and processing electronics [19, 20] located on the limbs. For a similar requirement, the coupling elements may permit a simplification in which the limbs of the antenna could be entirely passive, if a small addition, e.g. ~ 0.3 dB, to the noise figure of the extreme antenna element were to be permitted.

The TerraSAR-L mission [21] foundered because it was too expensive. An affordable, yet better performing variant of TerraSAR-L, using the coupling elements in a deployable DRA, in combination with centralised TRMs, DBF techniques and a low-cost launcher is worth a study.

SAOCOM-CS is a passive companion to SAOCOM for single-pass L-band SAR interferometry. It represents a new ESA mission concept that uses novel radar measurements (tomography, bistatic and specular) and

processing techniques for applications such as forest structure and biomass, surface motion detection, land cover and soil moisture [22]. When the planar transmission line coupling element technology is sufficiently mature, it may suit the system requirements of such missions.

7.5. S-band

Mobile satellite broadcast services address both the Digital Audio Radio Service (DARS) and Digital Multimedia Broadcasting (DMB). Missions currently use very large reflectors with aperture sizes in the range of 4m to 12m. Potentially, the coupling elements are applicable to either an array-fed reflector (AFR), using a deployable feed for illuminating the reflector, or in a DRA to replace the reflector.

CubeSats are being proposed for many future applications, including science, communications, Earth observation and technology demonstration. CubeSats usually employ VHF and UHF communication, which severely limits the transmission data rate. High-performance antennas for CubeSats are challenging due to their small physical dimensions. Nevertheless, an S-band antenna, utilising microstrip patch radiators on deployable panels, inter-connected by means of the coupling elements described herein, may be a feasible way of increasing the data transmission rate. Other applications may include its use in an extendable boom to carry antennas for interferometry.

NovaSAR-S [23], operating at 3.1 to 3.3 GHz, uses a non-deployable microstrip patch phased array (3m x 1m). Passive companions to NovaSAR-S, using the coupling elements in DRA antennas deployed from smaller satellites, could possibly be used in low-cost multi-static SAR missions.

7.6. Frequencies above 4 GHz

The higher losses in planar transmission lines at frequencies above 4GHz make the use of active arrays employing TRMs essential for meeting mission requirements. The effective use of the coupling elements is more restricted at these frequencies.

8. FUTURE WORK

Funding and interested parties are being sought to support design, development and test activities for progressing the Technology Readiness Level (TRL) [24] of the coupling elements technology. The foreseen activities are:

- Development of refined models to investigate and understand the electrical and mechanical behaviour, e.g. based on the FEM.

- Design, development and test of breadboard models for evaluating the electrical and mechanical performance.
- Assessment and verification of performance parameters, e.g.:
 - S-parameters
 - Amplitude and phase stability
 - Passive intermodulation
 - Multipaction
- Assessment of manufacturing tolerances on the performance parameters.
- Viability assessment of the technology and of its perceived benefits in future missions.

9. CONCLUSION

Preliminary computations indicate that the coupling elements, when used in conjunction with low-loss planar transmission line as described herein, could offer an alternative improved BFN technology. Funding is being sought to support design, development and test activities on different types of coupling element, in microstrip and stripline form, to progress the TRL of the new technology and to assess its suitability for use in deployable DRAs and other antennas in low frequency space missions. Successful implementation of the proposed coupling elements could bring benefits of high antenna efficiency, improved stability of amplitude and phase, low PIM, low deployment torque and possibly lower overall system mass. Lower BFN losses should allow a centralised location of electronic subsystems to help facilitate a cost-effective application of the DBF technique, bringing many advantages to future SAR and telecommunication space missions.

10. REFERENCES

1. Mangenot, C., Imbriale, W.A., (2012). Space Antenna Challenges for Future Missions, Key Techniques and Technologies. *Space Antenna Handbook*, Wiley Publication.
2. Davidson, M., Thompson, A. & Lin, C-C., (2008). Candidate Earth Explorer Core Missions - Reports for Assessment: BIOMASS, ESA SP-1313/2. ESA Communication Production Office, European Space Agency, Noordwijk, The Netherlands.
3. Bayrak, M., Eng, M. & Benson, F.A., (1975). Intermodulation Products from Nonlinearities in Transmission Lines and Connectors at Microwave Frequencies, *Proc. IEEE*, 122 (4).
4. Arazm, F. & Benson, F.A., (1980). Nonlinearities in Metal Contacts at Microwave Frequencies, *IEEE Transactions on Electromagnetic Compatibility*, EMC-22 (3).

5. Mangenot, C., (2008). Antenna: Needs and Technologies, Online at <https://escies.org/download/webDocumentFile?id=48502> (as of 31 August 2015). *European Space Components Information Exchange System*
6. Thompson, A. et al, (2008). A Stepped-Aperture Antenna Concept for Low Frequency SAR Missions, *Proceedings of the 30th ESA Antenna Workshop on Antennas for Earth Observation, Science, Telecommunication and Navigation Space Missions*. 415-418.
7. Thompson, A. & Thompson, M.S., (2011). Deployable Panel Structure for an Array Antenna, US Patent No. 8,035,573B2.
8. Thompson, A. & Thompson, M.S., (2012). Deployable Panel Structure, UK Patent No. GB2455311B.
9. Thompson, A. & Thompson, M.S., (2015). Deployable radio frequency transmission line, Patent Application No. GB1507353.9, *Intellectual Property Office Patents Journal*.
10. Ragan, G.L., (1948). Microwave Transmission Circuits, *Radiation Laboratory Series*, 9, McGraw_Hill Book Co., Inc.
11. van Berkel, S.L., et al., (2015). Characterization of printed transmission lines at high frequencies, *The 9th European Conference on Antennas and Propagation* (EuCAP 2015).
12. van Berkel, S.L., (2015). Characterization of Printed Transmission Lines at High Frequencies, MATLAB Software Tool. On line at <http://terahertz.tudelft.nl/Research/project.php?id=74&> (as of 31 August 2015). Delft University of Technology.
13. Montesano, A., et al. (2012) Microstrip Array Technologies for Space. *Space Antenna Handbook*, Wiley Publication.
14. Chen, Y., (2014). AIS and its Comparison with LRIT. *TransNav, the International Journal on Marine Navigation and Safety of Sea Transportation*. Vol. 8, No. 2.
15. Herige, A., et al., (2001). Antarctic Ice Sheet Sounding by Nadir Looking P-band Radar. CEOS-SAR01-007, *CEOS-SAR Workshop Proceedings*, National Space Development Agency of Japan (NASDA) Earth Observation Research Center (EORC).
16. Fletcher, K. (2012). Report for Mission Selection: Biomass, ESA SP-1324/1. ESA Communication Production Office, European Space Agency, Noordwijk, The Netherlands.
17. Saameno Perez, P. & Ludwig, M., (2008). Advanced digital beamforming architecture for synthetic aperture radar. *Proceedings of the 30th ESA Antenna Workshop on Antennas for Earth Observation, Science, Telecommunication and Navigational Space Missions*. 427-430
18. Martín-Neira, M., (1993) A Passive Reflectometry and Interferometry System (PARIS): application to ocean altimetry, *ESA Journal*, **17**:331–355.
19. Martín-Neira, M., et al., (2002). The MIRAS Demonstrator Pilot Project. *ESA Bulletin*, **111**, 123-131.
20. Drinkwater, M., et al. (2009) Star in the sky. The SMOS payload: MIRAS. *ESA Bulletin*, **137**, 16–22.
21. Simpson, D.M., Burbidge, G.T.A., Thornbury, A. & Ghinelli, B., (2004). TerraSAR-L System. *Proc. SPIE 5236, SAR Image Analysis, Modeling, and Techniques*, Vol. 17.
22. Davidson, M.W.J., (2014). SAOCOM-CS: A passive companion to SAOCOM for single-pass L-band SAR interferometry. *Belgium Earth Observation Day*.
23. Whittaker, P., Cohen, M., Hall, D., Gomes, L., (2011). An Affordable Small Satellite SAR Mission, *8th IAA (International Academy of Astronautics) Symposium on Small Satellites for Earth Observation*, Berlin, Germany,
24. TEC-SHS, (2008). *Technology Readiness Levels Handbook for Space Applications*.